Available online at www.sciencedirect.com

SCIENCE DIRECT®

Remote Sensing of Environment 103 (2006) 127–139

Remote Sensing of Environment

www.elsevier.com/locate/rse

Soil moisture mapping and AMSR-E validation using the PSR in SMEX02

Rajat Bindlish [a,*], Thomas J. Jackson [b], Albin J. Gasiewski [c], Marian Klein [c], Eni G. Njoku [d]

[a] SSAI, USDA ARS Hydrology and Remote Sensing Lab, 104 Bldg. 007 BARC-West Beltsville, MD 20705, United States
[b] USDA ARS Hydrology and Remote Sensing Lab, Beltsville, MD 20705, United States
[c] NOAA Environmental Technologies Lab, Boulder, CO, United States
[d] Jet Propulsion Lab, Pasadena, CA, United States

Received 26 December 2003; received in revised form 31 January 2005; accepted 5 February 2005

Abstract

Field experiments (SMEX02) were conducted to evaluate the effects of dense agricultural crop conditions on soil moisture retrieval using passive microwave remote sensing. Aircraft observations were collected using a new version of the Polarimetric Scanning Radiometer (PSR) that provided four C band and four X band frequencies. Observations were also available from the Aqua satellite Advanced Microwave Scanning Radiometer (AMSR-E) at these same frequencies. SMEX02 was conducted over a three-week period during the summer near Ames, Iowa. Corn and soybeans dominate the region. During the study period the corn was approaching its peak water content state and the soybeans were at the mid point of the growth cycle. Aircraft observations are compared to ground observations. Subsequently models are developed to describe the effects of corn and soybeans on soil moisture retrieval. Multiple altitude aircraft brightness temperatures were compared to AMSR-E observations to understand brightness temperature scaling and provide validation. The X-band observations from the two sensors were in reasonable agreement. The AMSR-E C-band observations were contaminated with anthropogenic RFI, which made comparison to the PSR invalid. Aircraft data along with ancillary data were used in a retrieval algorithm to map soil moisture. The PSR estimated soil moisture retrievals on a field-by-field comparison had a standard error of estimate (SEE) of 5.5%. The error reduced when high altitude soil moisture estimates were aggregated to 25 km resolution (same as AMSR-E EASE grid product resolution) (SEE ~ 2.85%). These soil moisture products provide a validation of the AMSR retrievals. PSR/CX soil moisture images show spatial and temporal patterns consistent with meteorological and soil conditions. The dynamic range of the PSR/CX observations indicates that reasonable soil moisture estimates can be obtained from AMSR, even in areas of high vegetation biomass content (~4–8 kg/m2).

Keywords: Microwave remote sensing; Soil moisture; AMSR; PSR

1. Introduction

The measurement of soil moisture is important for understanding the global hydrologic cycle and its effect on weather and climate. Soil moisture is a useful hydrologic parameter across all scales. On a global scale, soil moisture is important as a boundary condition for hydrologic and climate models. On a regional scale, it is important for agricultural assessment (crop yield models, drought prediction, etc.) and flood control. As important as it seems to our understanding of hydrology, soil moisture is a descriptor that has not had widespread application in the modeling of these processes (Engman & Gurney, 1991). There are two important reasons for this omission. First, soil moisture is a difficult variable to measure on a consistent and spatially comprehensive basis. The large spatial and temporal variability that soil moisture exhibits in the natural environment makes it difficult to measure and use in Earth Science applications. Secondly, the understanding of the role of soil moisture in hydrology and ecosystem processes has been

* Corresponding author. Tel.: +1 301 504 5363; fax: +1 301 504 8931.
E-mail address: bindlish@hydrolab.arsusda.gov (R. Bindlish).

0034-4257/$ - see front matter © 2005 Elsevier Inc. All rights reserved.
doi:10.1016/j.rse.2005.02.003

developed from point studies where the emphasis has been on the variability of soil moisture with depth. As a result, most models have been designed around the available point data, and do not describe the influence of spatial variability.

Global remote sensing of soil moisture has been a goal of research for the past two decades. Remote sensing of soil moisture can be accomplished using L-band (~1.4 GHz) microwave radiometry, as demonstrated in several experiments (Jackson et al., 1995; Jackson et al., 1999). Microwave observations at L-band provide reasonable penetration of crop vegetation canopy as well as provide measurements of soil moisture at soil depths of ~5 cm. The presence of water affects the bulk dielectric properties of soil and hence the emissivity of the soil surface. Atmospheric, vegetative and surface roughness properties also impact microwave emission. Frequencies in the L-band (~1.4 GHz) are preferable for soil moisture retrieval since these affects become more pronounced with an increase in frequency.

While recent advances now make the implementation of such a system in space a reality in this decade, there are currently new satellite sensors operating at somewhat higher frequencies that show promise for soil moisture mapping under some conditions (Njoku et al., 2003). Radiometry using higher microwave frequencies provides progressively less penetration of vegetation and soil probing depth, but is more amenable to implementation using current airborne or spaceborne antenna technologies and complement a wider range of applications. The Japanese AMSR-E imaging radiometer on board the NASA EOS Aqua satellite is one such sensor capable of retrieving soil moisture using a microwave channel at 6.9 GHz with ~60 km spatial resolution. Aqua was launched in May 2002, and will provide a global soil moisture product based on AMSR-E data in regions with low levels of vegetation (Njoku et al., 2003).

Soil moisture retrieval algorithms utilizing AMSR data have been proposed but not rigorously evaluated since there are few data sets available for this purpose (Bindlish et al., 2003; Jackson, 1993; Njoku & Li, 1999; Njoku et al., 2000; Paloscia et al., 2001). This is a critical issue that needs to be addressed for both algorithm development and validation. The Soil Moisture Experiment 2002 (SMEX02) was designed to provide data sets for these purposes. Ground observations of soil moisture and related variables were collected in conjunction with airborne measurements with the Polarimetric Scanning Radiometer with its C- and X-band scanheads (PSR/CX). PSR/CX has the same lowest frequencies as the AMSR instrument (6.92 and 10.7 GHz).

Aircraft data were processed to generate a series of calibrated, georegistered and temporally normalized brightness temperature (T_B) products. Low altitude observations are compared to ground estimates of field average soil moisture with a sampling depth of 0–6 cm. The sensitivity of T_B to soil moisture was evaluated for corn and soybeans providing new insights on the potential of these frequencies under significant vegetation biomass levels. High altitude observations of T_B were compared to AMSR-E T_B observations. Relationships between brightness temperature and soil moisture were analyzed to develop the soil moisture retrieval algorithm. This algorithm was used to map soil moisture over the entire region on each flight date.

2. SMEX02 description

Early soil moisture experiments (Washita 92, SGP97, SGP99) were conducted over areas with nominal vegetation water content (<2 kg m^{-2}). A soil moisture retrieval algorithm for C-band was rigorously tested across a wide range of soil moisture conditions during SGP99 under low to moderate vegetation (Jackson et al., 2002). Soil moisture experiment 2002 (SMEX02) was designed to extend the algorithm to areas under moderate to heavy vegetation water content conditions (4–8 kg m^{-2}).

Key objectives of the Soil Moisture Experiments 2002 (SMEX02) were to: 1) develop and validate soil moisture retrieval algorithms for agricultural conditions with high biomass levels for current (C Band) and future (L Band) passive and active microwave missions (e.g. SMOS, ALOS), 2) provide a link from point scale theory to integrated satellite footprint observations, 3) validate brightness temperature and soil moisture products developed from the Aqua Advanced Microwave Scanning Radiometer (AMSR-E), and 4) to understand land-atmosphere interactions under moderate to heavy biomass conditions. SMEX02 was conducted over a three-week period during the summer near Ames, Iowa, which is dominated by corn and soybeans.

One of the most important components of SMEX02 was the passive microwave aircraft program to support AMSR-E algorithm development and validation. The aircraft measurements provide a valuable link between the ground observations and the satellite measurements. A new version of the Polarimetric Scanning Radiometer was used in SMEX02 that provided four C band and four X band frequencies. High altitude flights were used to map a 50 by 100 km region on ten days over an 18-day period; six of these dates were concurrent with AMSR-E ascending overpasses. Low altitude flights were used to collect higher resolution data over thirty intensively sampled fields. SMEX02 was designed to provide early post-launch validation for AMSR-E on the EOS Aqua satellite.

The regional study area (IA) and the more intensively measured Walnut Creek Watershed (WC) are shown in Fig. 1. Details can be found in the experiment plan and website (http://www.ars.usda.gov/Research/docs.htm?docid=8993). As noted previously, ground, aircraft and satellite measurements of soil moisture were conducted.

The watershed is representative of the Des Moines Lobe, which covers approximately 1/4 of the state of Iowa. The climate is humid, with an average annual rainfall of 835 mm. The area around central Iowa is considered the pothole region of Iowa because of its undulating terrain. This area

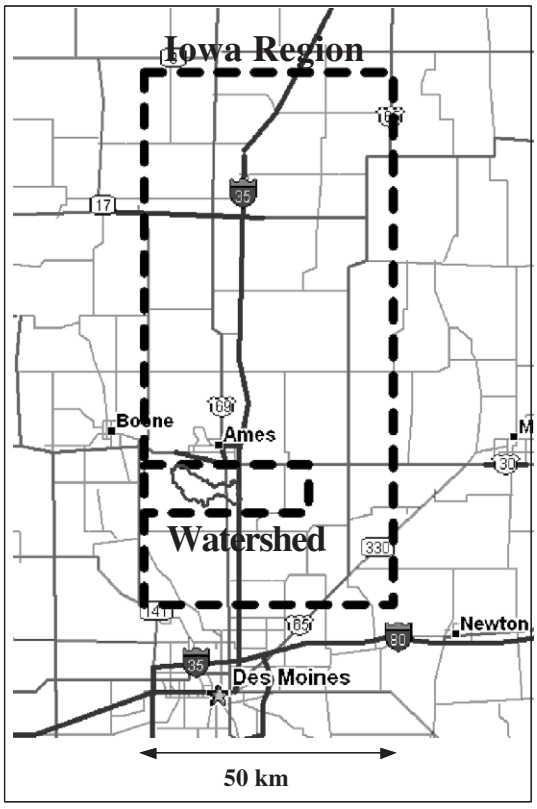

Fig. 1. Location of the SMEX02 experiment and Iowa regional (IA) and Walnut Creek Watershed (WC) sampling areas.

on the Des Moines Lobe represents the youngest of soils in the United States. Due to the presence of the potholes, this area has a large variation of soil types within a field. Surface organic matter contents often range from 1%–2% to over 8% in a transect from the pothole areas to the eroded knolls within the same field. This is also coupled with a variation in rooting depth. Typically, these potholes are dry by early spring due to subsurface drainage. The topography is characterized by low relief and poor surface drainage.

Two different approaches were adopted for ground based soil moisture measurements. Extensive soil moisture sampling was done in the Walnut Creek watershed area. The goal of soil moisture sampling in the watershed sites was to provide a reliable estimate of the mean and variance of the volumetric soil moisture for the fields that are approximately 800 m by 800 m. These measurements were used to validate the aircraft based microwave estimates at the field scale. Forty-two theta probe (TP) samples at 14 different locations and 4 gravimetric soil moisture (GSM) samples (coincident with 4 theta probe locations) were taken in every field. The gravimetric measurements of 0–6 cm were made with a coring tool, which also provided a reliable estimate of bulk density. The theta probe observations with a sampling depth of 0–6 cm were calibrated using the gravimetric observations taken in the field to estimate soil moisture. The average of the calibrated theta probe measurements were used as a field average. Soil moisture sampling was also done at a larger scale (satellite foot-print scale) to provide a reliable estimate of volumetric soil moisture for validating satellite observations. Forty-seven sampling sites located along 4 North–South transects with 12 sampling sites each (one of the transects had 11 sites) were sampled each day that covered a domain of approximately 50 km by 100 km (Fig. 2). At each of these sites three theta probe and one gravimetric soil moisture observations were made. The average of the calibrated theta probe observations was used as a field average for the sampling site. Further details can be found in the experiment plan and website (http://www.ars.usda.gov/Research/docs.htm?docid=8993).

Nearly 95% of the region and watershed is used for row crop agriculture. Corn and soybean are grown on approximately 90% of the row crop acreage. Approximately 60% of the crop was corn and 40% soybeans. Fig. 2 shows the Landsat imagery on July 1, 2002 over the study area. During the study period (June 6–July 12, 2002) the vegetation water content of corn increased from approximately 0.5–8 kg/m^2 over the region. Soybean vegetation water content increased from 0.2 kg/m^2 to 2 kg/m^2 of the data sets developed in SMEX02 (Jackson et al., 2004). The PSR observations were conducted (June

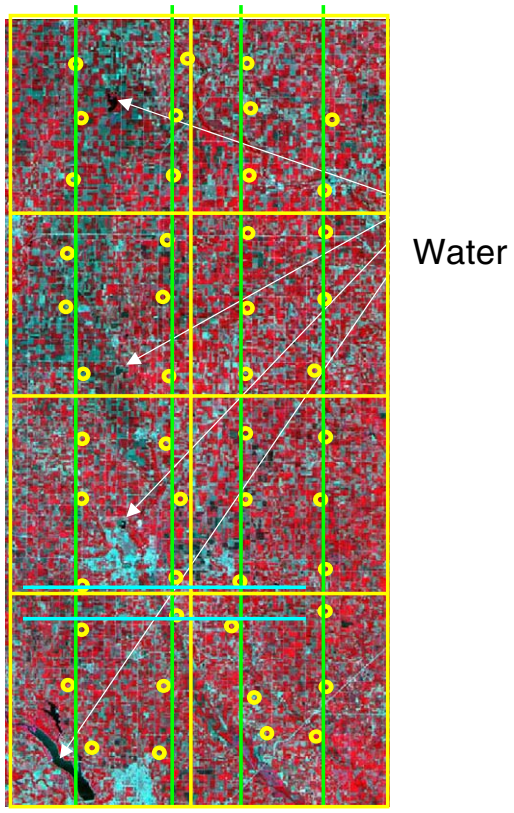

Fig. 2. Landsat TM7 false color image over the SMEX02 region on July 1, 2002 showing the presence of water bodies (white arrows). The regional sampling sites (yellow circles), regional (IA) flightlines (green lines), watershed (WC) flightlines (cyan lines) and the 8 EASE grid boxes (yellow boxes) are also shown in the figure. (For interpretation of the references to colour in this figure legend, the reader is referred to the web version of this article.)

25–July 12, 2002) during peak biomass conditions (corn—4.0–8.0 kg/m^2, soybean 1.0–2.0 kg/m^2).

3. Advanced Microwave Scanning Radiometer (AMSR-E)

The Advanced Microwave Scanning Radiometer (AMSR-E) (Njoku et al., 2003) was developed by the Japan Aerospace Exploration Agency (JAXA) and launched on board the National Aeronautics and Space Administration (NASA) EOS Aqua satellite on May 4, 2002. A sister instrument, the AMSR on the Japanese ADEOS-II satellite, was launched in December 2002. Early examinations of AMSR-E instrument data have shown evidence of extensive Radio-Frequency Interference (RFI) in the 6.9-GHz brightness temperature measurements (Li et al., 2004). AMSR-E makes dual-polarized passive microwave measurements at six frequencies: 6.9, 10.7, 18.7, 23.8, 36.5, and 89 GHz. From the 705-km Aqua orbit the antenna nadir angle of 47.4° provides an Earth incidence angle of 55°. The antenna beams scan conically about the nadir axis. The ±61° active portion of the azimuth scan angle provides an observation swath width of 1445 km. The orbit is Sun-synchronous with equator crossings at 1:30 pm and 1:30 am local solar time. Additional details of the radiometer and antenna characteristics are listed in Njoku et al. (2003).

The C (6.9 GHz) and X-band observations (10.7 GHz) have great potential for soil moisture estimation. Atmospheric effects at these frequencies are minimal and it is possible to partially filter the effects of vegetation and surface roughness on the brightness temperature observations through relatively simple radiative transfer modeling (Jackson, 1993). AMSR-E observations are available globally with a relatively short (2–3 days) repeat time and will form the basis for the first globally available daily soil moisture product (Njoku et al., 2003). Standard soil moisture products are a goal of both the NASA Aqua AMSR-E science team (Njoku et al., 2003) and the Japanese ADEOS-II AMSR program (Koike et al., 2000). At the present time both programs are refining and validating algorithms. In addition, the Navy Windsat Coriolis sensor is currently collecting similar data. WindSat data would enhance soil moisture mapping with alternative observing times (with respect to AQUA AMSR-E) and increased temporal coverage.

It is hoped that the availability of these products will spawn new applications for remotely sensed soil moisture. However, hopes for AMSR-E soil moisture products have been tempered somewhat by the discovery that microwave measurements at C-band frequencies are highly susceptible to man-made radio frequency interference (RFI). The AMSR-E C-band radiometer makes observations with a central frequency of 6.925 (350 MHz bandwidth) that is shared with fixed and mobile communication services and is subject to RFI contamination—particularly near large urban areas (Njoku et al., 2003). Very little RFI has been reported in other AMSR-E channels.

4. Polarimetric Scanning Radiometer (PSR)

The PSR is an airborne microwave imaging radiometer operated by the NOAA Environmental Technology Laboratory (Piepmeier & Gasiewski, 2001) for the purpose of obtaining polarimetric microwave emission of the Earth's oceans, land, ice, clouds, and precipitation. It has been successfully used in several major experiments including SGP99 (Jackson et al., 2002).

The PSR/CX scanhead houses two thermally stabilized polarimetric radiometers that share a common dual-band lens/feedhorn antenna. Each radiometer has four sub-bands that provide sensitivity to both vertical and horizontal polarization, along with an analog correlator that provides sensitivity to the third and fourth Stokes parameters at each of the two primary bands. The radiometers use internal noise diodes for rapid pre-calibration, along with external views of hot and ambient blackbody targets and cold space to provide absolute radio thermal calibration.

The PSR/CX radiometers are scanned in a conical mode using a gimbal drive mechanism (the PSR 'positioner'). The positioner rotates the scanhead as fast as one rotation in ~2.7 s. This rotation rate along with an 18 msec sample period provides near-Nyquist sampling of the scene below the aircraft at 1200 m above mean sea level, and Nyquist sampling at 8200 m above mean sea level. The sensitivity of the radiometers is better than 1 K for 18 msec integration time at most of the PSR/CX sub-bands.

The scanhead is rotatable by the positioner so that the radiometers can view any angle within ~70° elevation of nadir at any azimuthal angle, as well as external hot and ambient calibration targets. The configuration thus supports conical, cross-track, along-track, fixed-angle stare, and spotlight scan modes. Conical scanning at 55° incidence from nadir was used in SMEX02.

The PSR/CX system provided simultaneous four-Stokes' vector measurements within four adjacent frequency sub-bands in both C-and X-bands (Table 1). The multiband

Table 1
PSR/CX channels for SMEX02

Frequency (GHz)	Frequency band (GHz)	Polarizations	Beamwidth (°)
6.00	5.82–6.15	v, h	10
6.50	6.32–6.65	v, h	10
6.92	6.75–7.10*	v, h, U, V	10
7.32	7.15–7.50	v, h	10
10.64	10.63–10.65	v, h	7
10.69	10.68–10.70	v, h	7
10.70	10.6–10.8*	v, h, U, V	7
10.75	10.74–10.76	v, h	7
Thermal	9.6–11.5 um	–	7

* Indicates close to an AMSR-E channel.

capability of PSR/CX allows the study of using frequency agile radiometry for observations over interference prone regions. The primary lens/feedhorn antenna is located adjacent to a co-boresighted video camera and longwave (10 um) IR sensor.

Calibration of all radiometers was performed in-flight using standard (unpolarized) hot and cold blackbody targets. During SMEX02, the PSR/CX scanhead was integrated into the NASA Wallops Flight Facility (WFF) P-3 B aircraft in the aft portion of the bomb bay. Spatial resolution and other features of the PSR/CX are listed in Table 1.

5. Aircraft data collection and processing

The P3-B flights were flown during the mid day in order to match the nominal Aqua overpass time of 1400 (local standard time). Each flight was approximately 2 h in duration. The aircraft missions were scheduled to collect data over the Watershed area first and then over the Region (Fig. 1). The Regional data collection period was centered on the Aqua satellite overpass time of approximately 2:00 pm local standard time (CST). The SMEX02 campaign included two East-West low altitude flightlines over the Walnut Creek Watershed (WC) and four North-South high altitude flightlines over the Regional area (IA) designed to provide brightness temperature imagery (Table 2). The location of the flight lines is shown in Fig. 2. Data were collected on a total of ten days, six with Aqua AMSR-E coverage. A complete summary of the PSR and AMSR-E coverage on different dates is provided in Table 3.

5.1. Removal of RFI and channel selection

An initial review of the PSR/CX data for all the C-band frequencies available indicated that anthropogenic radio frequency interference (RFI) was present in all channels and both polarizations. RFI is manifested by higher than expected brightness temperatures (T_B), sometimes exceeding the nominal geophysical brightness temperatures by hundreds of Kelvins. In most cases the RFI was spatially localized, temporally consistent and often present in all channels simultaneously.

Table 2
PSR flightline and mapping specifications for SMEX02

Location	Regional	Watershed
Altitude (AGL) in m	8000	1500
Number of flight lines	4	2
Flight line length (km)	115	31
Flight line spacing (km)	11	3.3
Swath width (km)	19	4.75
Scan period (s)	3	3
Incidence angle (deg)	55	55
Nominal local time	12:45–15:00	12:00–12:30
3-dB footprint resolution	3.0 km at 6 GHz	630 m at 6 GHz
	2.0 km at 10 GHz	440 m at 10 GHz

Table 3
PSR SMEX02 data sets

Date	Lines	Aqua coverage	Comments
June 25	All	Yes	
June 27	All		
June 29	All	Yes	
July 1	All		
July 4	All	Yes	
July 8	All	Yes	Late
July 9	All	Yes	
July 10	All		
July 11	All	Yes	
July 12	All		Early

The purpose of using multiple sub-bands for each primary PSR/CX band is to provide a means of detecting anthropogenic radio frequency interference. Such an interference detection and correction algorithm was successfully demonstrated using PSR data from the 1999 Southern Great Plains Experiment (SGP99) (Gasiewski et al., 2002). The algorithm works by comparing brightness temperatures in several nearby sub-bands through the use of a standard spectral model. It is possible to correct for RFI which has a narrow band-width and thus effects the brightness temperature observations in a few bands only. This methodology does not correct for the presence of wide spread RFI over the entire spectrum. If the observed brightness temperature is above acceptable observations (320 K in this case) then it is flagged as RFI.

As anticipated, interference was also observed during the SMEX02 experiment over Iowa, particularly in the AMSR-E 6.925 GHz band. The PSR/CX sub-bands were used to identify the general location of the interference and to select the frequency band of least contamination. Relatively few occurrences of interference were noted at X-band.

Based upon a close examination of the RFI in the data, we concluded that the 7.32 GHz and 10.7 GHz bands were far superior to the others. Therefore, all analyses will only consider these channels.

5.2. Temporal normalization

Collecting high resolution radiometric data over a large region requires considerable aircraft flight time. For SMEX02, it took approximately 2 h to complete a mapping session on any given day. During this time interval, both the surface emissivity and physical temperature increased during the course of the flighttime. Other long term drifts in instrument characteristics not accounted for in the calibration process could have also caused some brightness temperature variations over the flight period.

By design, the data from any given flight line overlapped somewhat the data from adjacent flight lines. Since we wish to have the equivalent of an instantaneous snapshot of the region, it was necessary to normalize the observed imagery to a single time. It is assumed that no temporal correction was needed within a given flight line, but rather only from

line to line. Next, the second of the four north–south lines on each day was used as a standard for that day. All data points that fell in the overlapping areas of the flight lines were identified and averaged by line. The average of this area for each line was compared to the same area for line 2 to determine a correction offset. This correction offset, independent of the location on the flightline, was used for all the observations on that line. This technique has been employed in previous aircraft missions (Jackson et al., 2002).

6. Comparison of AMSR-E and PSR brightness temperatures

One of our goals in SMEX02 was to provide a validation over land of the brightness temperature products generated from Aqua AMSR-E. This analysis also addresses an important science question; do the high resolution aircraft T_B data scale directly to the coarse resolution satellite observations?

The dates on which concurrent satellite and aircraft observations were available were June 25 and 29, and July 4, 8, 9 and 11, 2002. PSR brightness temperature observations at 7.32 GHz and 10.7 GHz were averaged over the regional domain (~80,000 PSR footprints). Average T_B values were also computed for AMSR-E observations for both 6.925 GHz and 10.7 GHz frequency channels. The results indicated that the AMSR-E calibration and PSR calibration at X-band (10.7 GHz) for both V and H polarizations are nominally the same (Fig. 3). This indicates a good calibration of the AMSR-E channels, assuming that the PSR was well calibrated during the SMEX02 campaign. The agreement between the average of the coarse resolution AMSR-E observations and high resolution PSR observations at X-band also supports the assumption that scaling is linear. The 6.9 GHz data for the Iowa Region had RFI contamination, whereas the aircraft data had only minor contamination. The C-band results clearly indicate a significant bias (AMSR-E > PSR), due to the presence of RFI contribution (Fig. 3). The AMSR-E observed brightness temperature at C-band is about 15K higher than the PSR observations. This difference in observations is observed on all the days at both H and V polarizations. The SMEX02 sampling domain included areas with and without presence of significant RFI. The change in observed T_B on different dates is due to changes in areas not affected by RFI. The response of the dielectric constant at C-band is constant over the range of frequencies. The change in geophysical response over the C-band (6.5 GHz-7.3 GHz) is small and is within the noise levels of the instrument. The presence of multiple sub-bands in PSR/CX at C-band provided an opportunity to develop mitigation measures against RFI. The presence of RFI in C-band AMSR observations raises questions about the reliability of soil moisture estimates made using these observations.

7. Soil moisture retrieval algorithm

The relationship between brightness temperature (T_B) and soil moisture, surface roughness and vegetation water content is nonlinear. The algorithm for deriving soil moisture and temperature from TMI observations is based on physical models of microwave emission from a layered soil–vegetation–atmosphere medium. Atmospheric effects were assumed to be minimal for this study. A soil moisture retrieval algorithm similar to that as described in (Jackson,

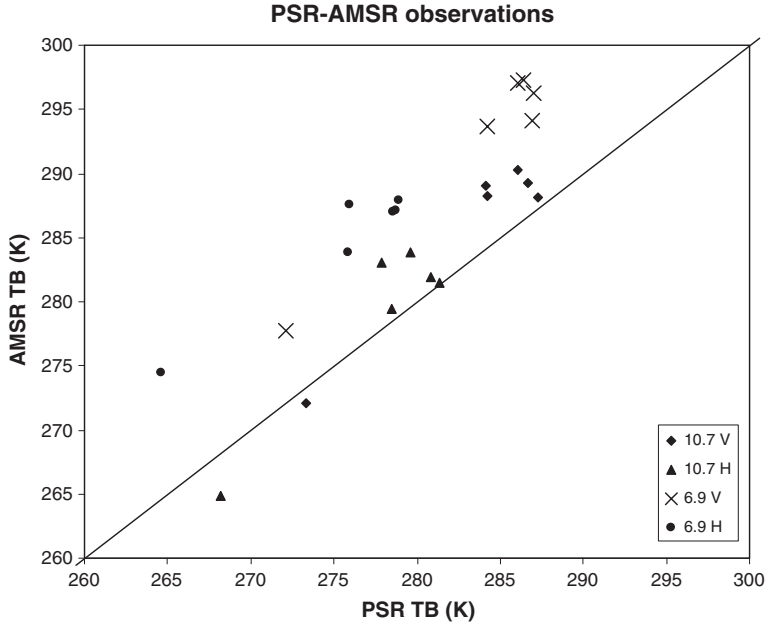

Fig. 3. Comparison between daily PSR and AMSR-E C-and X-band observations averaged over the regional sampling area during SMEX02.

1993) was developed. Surface emissivity (e_s) is calculated by dividing the brightness temperature (T_B) by the soil surface temperature (T_S). The pixel emissivity is corrected for vegetation using the approach proposed by (Jackson & Schmugge, 1991). In this approach the vegetation is treated as an attenuating layer with transmissivity (γ) that depends on the vegetation optical depth (τ) and the incidence angle (θ). A semi-infinite soil layer of physical temperature T_e, an air-soil reflectivity r, and a layer of vegetation of physical temperature ($T_e = T_s$) was proposed. The resulting equation used is:

$$T_B = eT_e\exp(-\tau) + T_c(1-\alpha)[1-\exp(-\tau)] \times [1 + r\exp(-\tau)] \quad (1)$$

where e and r are the emissivity and reflectivity of the soil surface and α is the single scattering albedo of vegetation.

The optical depth of the canopy is determined using a first-order approximation of the vegetation parameter (b), which is a function of land use, and vegetation water content (VWC):

$$\tau = b^{*}\mathrm{VWC}\,. \quad (2)$$

The effect of surface roughness (s) on soil reflectivity (r') can be characterized by (Choudhury et al., 1979)

$$r' = r\exp\left(-h\cos^2\theta\right) \quad (3)$$

where h is a roughness parameter ($=4s^2k^2$), i.e., proportional to the root mean square (RMS) height variations of the soil surface, and $k = 2\pi/\lambda$.

The effective dielectric constant of the surface layer is computed by inverting the Fresnel equations. Finally, the dielectric mixing model (Wang & Schmugge, 1980), which is based on soil texture, was used to estimate volumetric soil moisture at each pixel. A fixed value of 0.1 was used for surface roughness.

The algorithm in its current form requires several ancillary data sets for implementation: surface soil texture, land cover, and Normalized Difference Vegetation Index (NDVI). The following summarizes the decisions and datasets selected for this process.

7.1. Surface soil texture

Soil properties do not usually change quickly and, therefore, this data plane of ancillary data is considered constant. A multi-layer soil characteristics data set for the state of Iowa has been developed by Iowa State University (Iowa Soil Properties and Interpretations Database-ISPAID 6.0) which was adapted for this work (http://extension.agron.iastate.edu/soils/SSDS_maps.html).

7.2. Soil temperature

Soil Temperature measurements at 1 cm, 5 cm, and 10 cm were made daily at all the sampling sites during the experiment. The 5 cm measurements were interpolated at the mapping resolution.

7.3. Land cover

Land cover over the mapping domain was estimated using the Landsat imagery (Doriaswamy et al., 2004). Land cover is used in the algorithm to determine the vegetation parameter (b) and the single scattering albedo (α) for corn and soybean.

7.4. Vegetation parameter (b) and single scattering albedo (α)

The vegetation parameter (b) was estimated using the Land cover data. Vegetation parameter and single scattering albedo were assigned based on the high resolution (30 m) land cover data. A constant value was used for corn ($b = 0.174$ and $\alpha = 0.04$) and soybean ($b = 0.438$ and $\alpha = 0.07$) (Jackson & O'Neill, 1990). This was then aggregated to 200 m for watershed mapping and 800 m for regional mapping.

7.5. Vegetation water content

Vegetation water content was estimated using the high resolution Landsat imagery on a weekly basis. These weekly values were interpolated to obtain daily estimates of vegetation water content (Jackson et al., 2004).

8. Low altitude comparisons of brightness temperature and soil moisture

Field-by-field observations of brightness temperature were extracted for the sampling sites using the low altitude high resolution data. The PSR footprint for the low altitude flights during SMEX02 was ~630 m, which was smaller than the size of the sampling fields (~800 m). If ~90% of the PSR footprint was inside the field boundaries, the observations were used in computing the field average. PSR brightness temperature observations were averaged for every site. Fig. 4 shows the relationship between observed soil moisture and emissivity for a typical corn (WC20) and soybean field (WC09). This illustrates the sensitivity of C-band observations to soil moisture in the presence of high vegetation biomass. The presence of sensitivity in the emissivity and soil moisture observations even in areas of high vegetation water content (~4–8 kg/m^2) enables a reliable estimate of soil moisture.

The scatter plot of the observed soil moisture and the PSR estimated soil moisture for all the sampling sites for the duration of the experiment is shown in Fig. 5. The standard error of estimates of PSR estimated soil moisture for both corn (SEE = 0.052) and soybean (SEE = 0.061), which are as expected to be higher than in previous low level vegetation

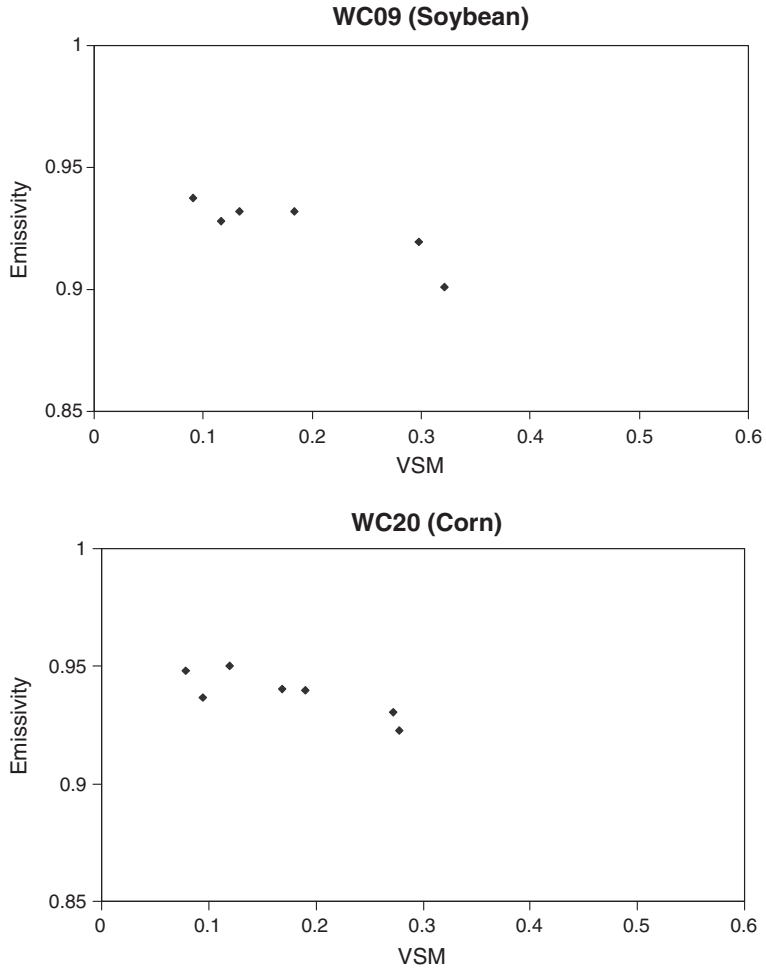

Fig. 4. Relationship between field scale observed volumetric soil moisture and PSR observed emissivity for a typical soybean (WC09) and corn (WC20) field.

studies. It is possible that some of the error in soil moisture estimation may be due to the contamination as a result of the mixed land cover in a pixel. Also, uniform values of the vegetation parameter and single scattering albedo were used for all corn and soybean fields, irrespective of their growth stage. This is likely to be an over simplification, but there are no studies that provide information on the dependence of the vegetation parameter on the plant phyenology. There were significantly higher soil moisture observations in the cornfields than the soybean fields, which could have contributed to a smaller error for the cornfields. The overall error for both the corn and soybean fields was SEE=0.054.

The same algorithm was applied using the X-band observations for both the corn and soybean fields at the

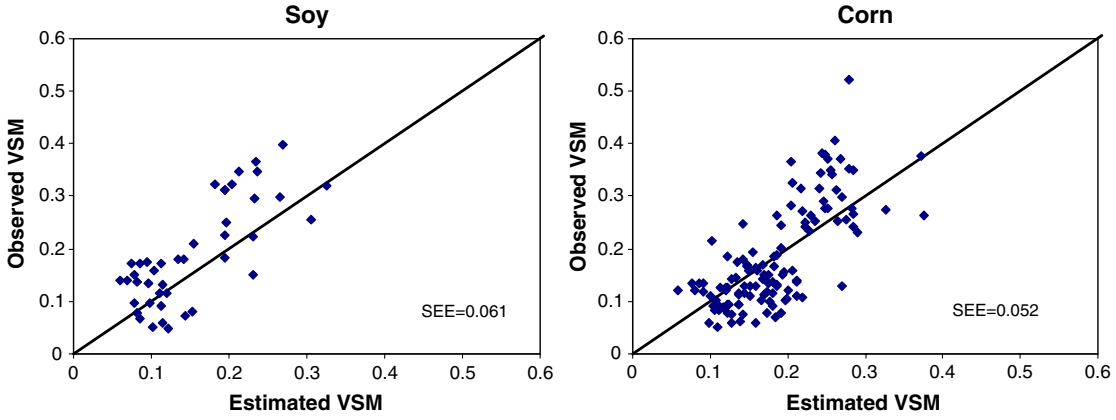

Fig. 5. Field scale evaluation of the C-band (7.32 GHz) PSR based single channel algorithm for all the corn and soybean fields in the watershed area. The overall standard error of estimate (SEE) was 0.054.

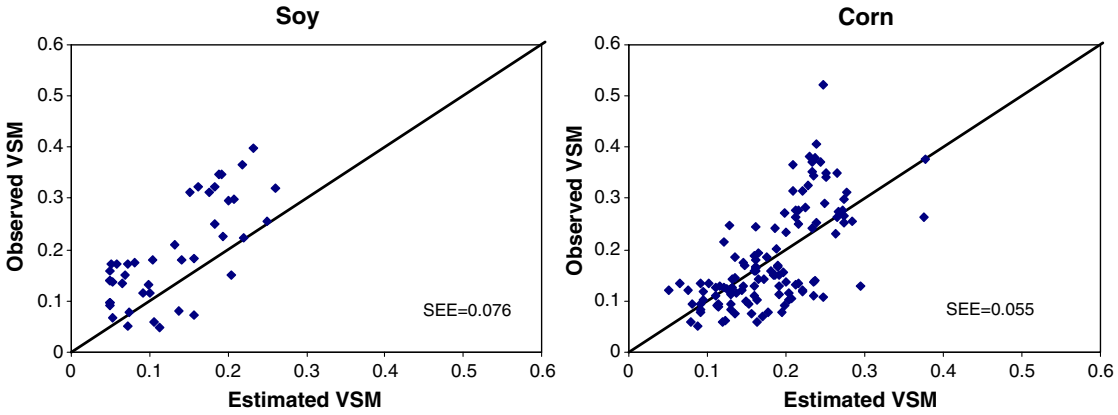

Fig. 6. Field scale evaluation of the X-band (10.70 GHz) PSR based single channel algorithm for all the corn and soybean fields in the watershed area. The overall standard error of estimate (SEE) was 0.061.

field scale. As expected, the standard error of estimates increased for both corn (SEE=0.055) and soybean (SEE=0.076) (Fig. 6). The overall error for all the sampling sites was SEE=0.061. Although the SEE for both corn and soybean were higher for the X-band observations, it does capture the soil moisture trend during the course of the experiment. This means that even with high levels of RFI in AMSR-E C-band observations, it would still be possible to obtain soil moisture estimates (though not very accurate) in vegetated regions.

9. High altitude mapping

The high altitude lines which have a nominal beam position spacing of 300 m were regridded at 800 m resolution. Fig. 7 shows the brightness temperature maps derived from the 7.32 H GHz observations over the regional sampling area. The brightness temperature images show distinct features which are consistent with the presence of water bodies and the meteorological conditions prevalent during the course of the experiment. Fig. 2 shows the

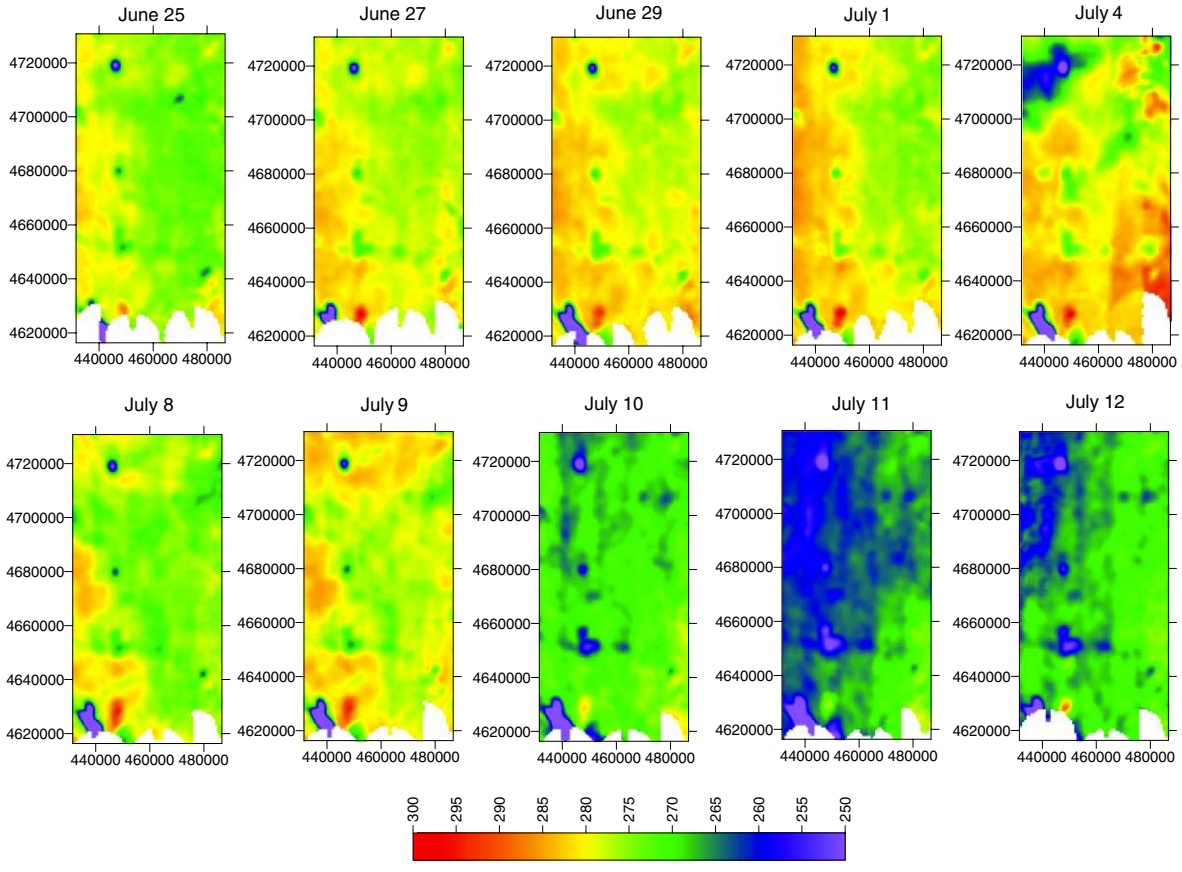

Fig. 7. PSR C-band (7.32 GHz) brightness temperatures observations over the regional area during SMEX02.

Landsat imagery from July 1, 2002 over the sampling area. The water bodies (4 in number) can be observed in all brightness temperature images.

The estimated soil moisture images are consistent with the expected patterns based upon precipitation. Fig. 8 shows the accumulated precipitation between two consecutive flight days. These brightness temperature observations were used with the single channel soil moisture retrieval algorithm to estimate soil moisture (Fig. 9). The conditions were relatively dry (~15 % soil moisture) at the onset of the SMEX02 experiment. There was no appreciable precipitation till July 4, and as a result the brightness temperature observations gradually increased over the sampling area until this occurred. The estimated soil moisture also shows a gradual dry-down (areal average of ~10% soil moisture) during his period.

A precipitation cell moved through the north-western part of the region on July 4, 2002 during the regional flights. The accumulated precipitation image for July 1–4 shows some precipitation in this area which was all received on July 4 concurrent with the aircraft observations. The soil moisture sampling within this area was cancelled due to this precipitation and only the areas which did not receive any precipitation were sampled. The PSR images show a significant drop in observed brightness temperature in this area. This is further illustrated in the soil moisture estimates for July 4.

The entire regional sampling area received significant precipitation (~25 mm) between July 4 and July 5. The next set of PSR observations were made on July 8, by which time the sampling domain was already in the middle of the dry-down. This resulted in lower brightness temperature observations throughout the regional sampling domain on July 8. These lower brightness temperatures resulted in higher soil moisture estimates throughout the sampling domain. The effect of July 4–5 precipitation event was limited in terms of soil moisture changes on July 8. There was no appreciable (less than 1 mm) precipitation on July 8–9, which resulted in higher brightness temperature observations and lower soil moisture on July 9 (as compared to July 8).

There was widespread heavy precipitation (~50 mm) throughout the sampling domain on the morning of July 10. This resulted in wet conditions through the sampling domain, which are reflected in lower brightness temperatures and higher soil moisture estimates. This was followed by more precipitation on July 10–11 (~20 mm). This resulted in very wet conditions with standing water in a number of sampling fields. The PSR observations show very low brightness temperatures throughout the sampling

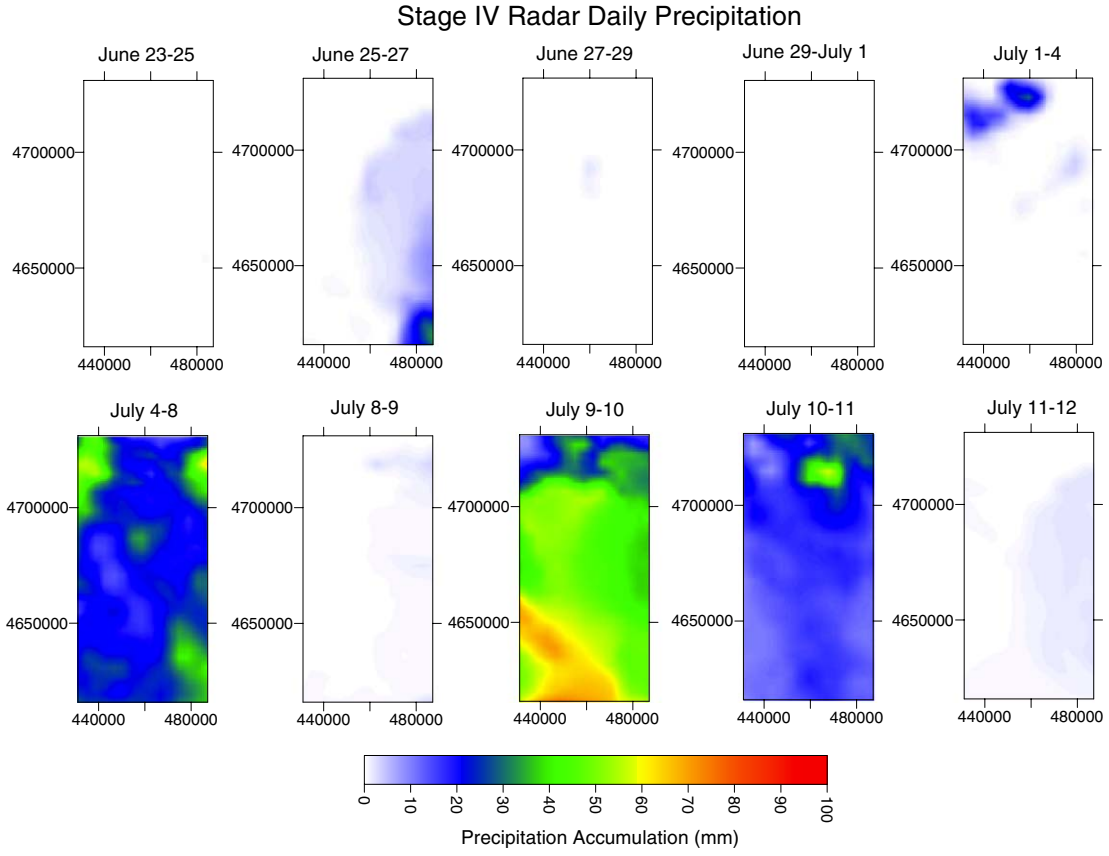

Fig. 8. Stage IV Radar estimates of accumulated precipitation between two consecutive PSR observations over the SMEX02 regional area.

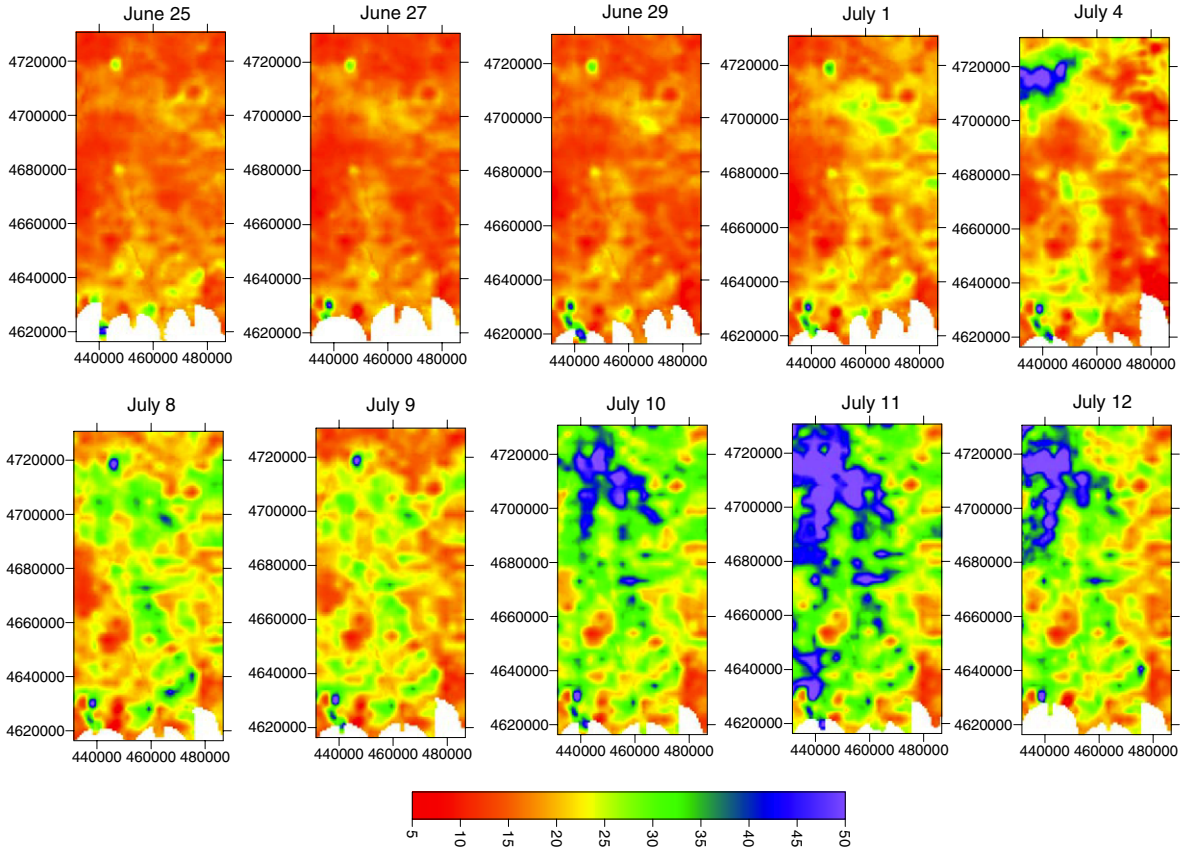

Fig. 9. Soil moisture estimates over the regional area using the C-band single channel algorithm during SMEX02.

domain. The soil moisture estimates illustrate these wet conditions. The last day of over flight (July 12) was not preceded by any precipitation. This resulted in the start of a slow dry down (lower soil moisture estimates on July 12 than July 11).

AMSR-E C-band brightness temperature has a coarse resolution of 60 km with a sampling frequency of 10 km. These observations are gridded in a regular 25 km grid (called EASE Grid). AMSR-E soil moisture estimates are made at this regular 25 km grid. The regional soil moisture

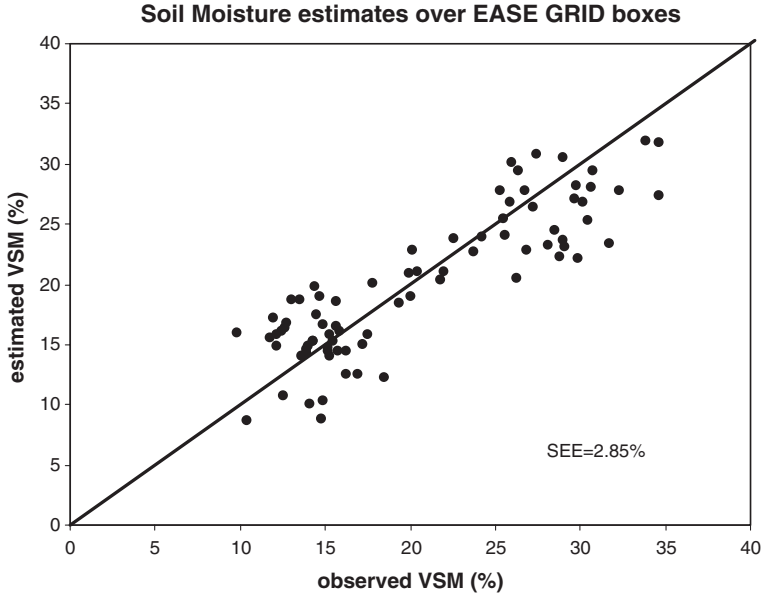

Fig. 10. Comparison between the observed soil moisture and PSR based soil moisture estimates over the EASE Grid boxes in the SMEX02 regional sampling area.

estimates were validated using the ground based regional soil moisture sampling. The soil moisture observations within each of the 8 EASE Grid boxes were averaged for each day and compared to the soil moisture estimates within the matching grid box (Fig. 10). Each EASE Grid box had 6 soil moisture sampling fields and approximately ~1200 PSR pixels at 800 m resolution. The PSR estimated soil moisture shows an excellent agreement with the observed soil moisture averages (SEE=2.85%). It was decided to omit the EASE Grid box in the north-west corner on July 4 due to ongoing rainfall. A similar analysis for the single channel X-band observations resulted in reasonable soil moisture estimates (SEE=3.56%). These results demonstrate the potential to retrieve and map soil moisture under vegetation conditions that we previously thought to be limiting at these frequencies.

10. Summary

AMSR-E observations at C-band will be used to estimate global soil moisture. PSR observations during SMEX02 provided an early validation dataset for calibration and validation of AMSR-E observations. The PSR/CX and its SMEX02 participation represent a significant contribution to algorithm development and validation. Comparison of similar X-band channels indicated reliable calibration. However, as expected the AMSR-E C-band channels were contaminated by RFI making the data useless for soil moisture in this region.

The vegetation conditions encountered during the experiment were close to peak biomass conditions (~8 kg/m^2). This provided a challenging algorithm validation dataset case condition. The soil moisture algorithm was evaluated using the ground based SMEX02 observations. Results obtained using the full soil moisture retrieval algorithm were good. At the field scale, the single channel algorithm resulted in unbiased estimates with a nominal error of 0.055, which was in the expected range. Regional estimates of soil moisture were consistent with the observed meteorological conditions. The errors dropped considerably when comparisons of soil moisture were made at a coarser resolution, consistent with satellite observations (~25 km) (SEE=0.0285). The additional error introduced by the use of X-band observations is minimal (SEE=0.0356), which is a significant contribution in the light of widespread areas of RFI contamination of AMSR observations at C-band. This can be useful in modifying operational soil moisture algorithms in these areas.

The results suggest that for vegetation conditions typical of the SMEX02 region that the soil moisture retrieval algorithm can be applied with confidence. However, these results clearly show that vegetation is a very significant factor when interpreting C-band brightness temperatures for soil moisture.

Aknowledgements

This work was supported by the National Aeronautics and Space Administration (NASA) EOS AMSR-E Instrument Science Program, NASA Terrestrial Hydrology Program, NASDA AMSR Science Program and the NOAA Office of Oceanic and Atmospheric Research.

References

Bindlish, R., Jackson, T. J., Wood, E., Gao, H., Starks, P., Bosch, D., et al. (2003). Soil moisture estimates from TRMM microwave imager observations over the southern United States. *Remote Sensing of Environment*, *85*, 507–515.

Choudhury, B.J., Schmugge, T.J., Chang, A., & Newton, R.W. (1979). Effect of surface roughness on the microwave emission from soils. *Journal of Geophysical Research*, *84*, 5699–5706.

Doriaswamy, P., Puegger, J., Hatfield, J., Stern, A., & Jackson, T. J. (2004). Land cover and crop yield estimation in the SMEX02 region. *Remote Sensing of Environment*, *92*, 548–559.

Engman, E. T., & Gurney, R. J. (1991). *Remote sensing in hydrology*. London: Chapman and Hall.

Gasiewski, A.J., Klein, M., Yevgrafov, A., & Leuskiy, V. (2002). Interference mitigation in passive microwave radiometry. *Proceeding int geoscience and remote sensing symp*, *vol. III*. (pp. 1682–1684) Toronto, CA: IEEE.

Jackson, T. J. (1993). Measuring surface soil moisture using passive microwave remote sensing. *Hydrological Processes*, *7*, 139–152.

Jackson, T. J., Chen, D., Cosh, M., Li, F., Anderson, M., Walthall, C., et al. (2004). Vegetation water content mapping using landsat data derived normalized difference water index (NDWI) for corn and soybeans. *Remote Sensing of Environment*, *92*, 475–482.

Jackson, T. J., Gasiewski, A. J., Oldak, A., Klein, M., Njoku, E., Yevgrafov, A., et al. (2002). Soil moisture retrieval using the C-band polarimetric scanning radiometer during the southern great plains 1999 experiment. *IEEE Transactions on Geoscience and Remote Sensing*, *40*, 2151–2161.

Jackson, T. J., Le Vine, D. M., Hsu, A. Y., Oldak, A., Starks, P. J., Swift, C. T., et al. (1999). Soil moisture mapping at regional scales using microwave radiometry: The southern great plains hydrology experiment. *IEEE Transactions on Geoscience and Remote Sensing*, *37*, 2136–2151.

Jackson, T. J., Le Vine, D. M., Swift, C. T., Schmugge, T. J., & Schiebe, F. R. (1995). Large area mapping of soil moisture using the ESTAR passive microwave radiometer in Washita '92. *Remote Sensing of Environment*, *53*, 27–37.

Jackson, T. J., & O'Neill, P. E. (1990). Attenuation of soil microwave emission by corn and soybean at 1.4 and 5 GHz. *IEEE Transactions on Geoscience and Remote Sensing*, *28*, 978–980.

Jackson, T. J., & Schmugge, T. J. (1991). Vegetation effects on the passive microwave emission of soils. *Remote Sensing of Environment*, *36*, 203–212.

Koike, T., Njoku, E. J., Jackson, T. J., & Paloscia, S. (in press). Soil moisture algorithm development and validation for the ADEOS-II/AMSR. *Proceedings of the int geoscience and remote sensing symposium, IEEE Catalog No. 00CH37120*, *vol. III*. (pp. 1253–1255).

Li, L., Njoku, E., Im, E., Chang, P., & St. Germain, K. (2004). A preliminary survey of radio-frequency interference over the U. S. in Aqua AMSR-E data. *IEEE Transactions on Geoscence and Remote Sensing*, *42*, 380–390.

Njoku, E. G., Jackson, T. J., Lakshmi, V., Chan, T. K., & Nghiem, S. V. (2003). Soil moisture retrieval from AMSR-E. *IEEE Transactions on Geoscience and Remote Sensing*, *41*, 215–229.

Njoku, E., Koike, T., Jackson, T. J., & Paloscia, S. (2000). Retrieval of soil moisture from AMSR data. In P. Pampaloni, & S. Paloscia (Eds.), *Microwave radiometry for remote sensing of earth's surface and atmosphere* (pp. 525–533). Utrecht, The Netherlands: VSP.

Njoku, E. G., & Li, L. (1999). Retrieval of land surface parameters using passive microwave measurements at 6 to 18 GHz. *IEEE Transactions on Geoscience and Remote Sensing*, *37*, 79–93.

Paloscia, S., Macelloni, G., Santi, E., & Koike, T. (2001). A multifrequency algorithm for the retrieval of soil moisture on a large scale using microwave data from SMMR and SSM/I satellites. *IEEE Transactions on Geoscience and Remote Sensing*, *39*, 1697–1707.

Piepmeier, J. R., & Gasiewski, A. J. (2001). High-resolution passive microwave polarimetric mapping of ocean surface wind vector fields. *IEEE Transactions on Geoscience and Remote Sensing*, *39*, 606–622.

Wang, J.R., & Schmugge, T.J. (1980). An empirical model for the complex dielectric permittivity of soils as a function of water content. *IEEE Transactions on Geoscience and Remote Sensing*, *18*, 288–295.